Aeroacoustic Assessment of Low-Observable UCAV Configurations

K.-S. Rossignol, S. Proskurov, M. Lummer, R. Ewert, J. W. Delfs
DLR – German Aerospace Center, Braunschweig
GERMANY

karl-stephane.rossignol@dlr.de

A. Kolb, S. Mancini
AIRBUS Defence and Space, Manching
GERMANY

ABSTRACT

First, results of experimental and numerical investigations on generic engine noise shielding by the SACCON UCAV configuration are presented. The results suggest that propulsion system intake noise is much less attenuated compared to exhaust noise. This is a consequence of the position of the intake on the symmetry plane of the UCAV as well as to the relatively large radius of curvature of the aircraft wings leading edge. This result emphasizes the potential necessity to achieve an acoustically optimized integration of both intake and exhaust altogether to maximize acoustic attenuation. The use of a generic, monopole-like, sound source in the experimental and numerical assessment of SACCON (Stability And Control CONfiguration) leaves many open questions with respect to the acoustic signature of a real UCAV configuration. For real highly-integrated propulsion systems, noise radiation from the intake and exhaust is critical to the acoustic detection of an aircraft, especially to low-observable configurations. Aiming at an assessment of the noise signature of a realistic UCAV configuration at an early design stage, experimental and numerical methodologies are presented which are able to account for mean flow and airframe interaction effects on noise generation and propagation. DLR-F24 MULDICON UCAV (MULti-Disciplinary CONfiguration) test bed is introduced, along with numerical simulations results providing first insights into the aeroacoustics of a realistic agile UCAV configuration.

1.0 INTRODUCTION

1.1 Motivation

As the potential issues related to the acoustic signature of UAV/UCAV gain in attention, there is an increased necessity to put efficient and accurate assessment methodologies in place. Although aeroacoustic simulation methodologies have been extensively validated and their state of development is mature, their application to UAV/UCAV configurations assessment is novel. Therefore, the aeroacoustic assessment of these vehicles is currently not part of the design chain, but comes as a by-product when the configuration is fixed. There is, therefore, a technological interest in the evaluation of current aeroacoustic prediction methodologies and their further development, with respect to UAV/UCAV applications. Specifically for UCAV, the advance of aeroacoustic simulation methodologies will lead to enhance capabilities in terms of low noise mission planning, minimizing the risk of early acoustic detection.

A central technical question, in term of the acoustic signature of UCAV, relates to engine integration. The actual position of the engine relative to an aircraft's planform directly impacts its acoustic signature, in part, through acoustic scattering (Smith 2012; Rossignol 2018; Rossignol 2016; Hutcheson 2014). Moreover, for jet-propelled vehicles, the specific characteristics of the exhaust jet, at the propulsion system exhaust, also have a strong impact on the vehicle's acoustic signature, in terms of absolute noise emission levels and directivity (Smith 2012; Papamos chou 2009). These effects are commonly referred to as installation effects.

The precise role of the high-velocity flow entering the intake of the propulsion system in defining the acoustic signature of the vehicle needs to be further investigated. Acoustic effects related to boundary layer ingestion as well as scattering at the intake also need to be taken into account by simulation for an optimized UCAV design (Rossignol 2018).

Further, the question of the integration of the propulsion system is not merely restricted to its placement relative to the UCAV planform, but also requires dealing with the geometrical design of the intake and exhaust ducts. This topic is highly relevant for infrared detection, which mostly drives the designs of curved intakes and exhausts for reduced heat signatures. This type of intake duct poses great challenges for engine design due to stronger flow non-uniformity upstream of the engine. The resulting impact of this kind of specialized configuration on the acoustic signature comes as a by-product requiring further investigation. Finally, aspects of noise mitigation could further help in reducing the acoustic signature of UCAVs. More specifically, the application of passive noise reduction devices has to be considered. The use of numerical simulation methods will help in specifying the design of such devices.

1.2 Previous efforts

As part of the NATO STO AVT-233 group, which dealt with the aeroacoustics of Engine/Rotor installation for Military Air Vehicles, the acoustic shielding properties of the SACCON UCAV (Stability And Control CONfiguration) planform were investigated. More specifically experiments were done, using a generic sound source, to quantify acoustic shielding by the airframe. The focus of the experiment was put on the quantification of the acoustic attenuation by the airframe as a function of engine placement i.e. source position. The main purpose of these tests was to put a database together, appropriate for the validation of aeroacoustic numerical simulation tools.

The source was deliberately kept highly generic (a monopole-like point source) to allow for a simple implementation in numerical prediction codes. However, the use of a generic acoustic source makes a transposition of the results to a realistic jet-propelled UCAV configuration difficult. It was also not possible to give attention to the actual details of the engine integration into the airframe, due to limitations of the wind tunnel model design. A quantification of the scattering of intake and exhaust noise was not possible as part of these experiments for the same reasons.

1.3 Aim

It is therefore intended, as part of NATO STO AVT-318 group (Low noise aeroacoustic design for turbofan powered NATO air vehicles), to pursue the work started on this topic to now deal with realistic sources on a concurrent agile (unmanned) NATO air vehicle design, the MULDICON UCAV configuration (MULti-Disciplinary CONfiguration), see Figure 8. In this contribution experimental and numerical results are presented aiming to review the current state of applicability of numerical simulation tools for the aeroacoustic assessment of the UCAV configurations. Furthermore, details of the planned wind tunnel experiment and model design are presented.

2.0 ACOUSTIC SHIELDING ASSESSMENT OF SACCON

In this section experimental and numerical simulation results for the acoustic shielding by the SACCON UCAV airframe are presented. The experimental methodology uses a generic monopole-like reference source to investigate the effect of source placement over the airframe on acoustic shielding. Comparisons between the experimental and numerical simulation results allow for an evaluation of the simulation method capabilities.

2.1 Numerical Method

The Fast Multipole Code for Acoustic Shielding (FMCAS) implements a high-frequency formulation of the multi-level Fast Multipole Method (FMM) based on a plane wave approximation of the free-field Green's function (Rahola 1998). The scattering surface is discretized using plane triangles with constant source strength. This requires a minimum resolution of 6 elements per wavelength. The iterative solvers are taken from the PETSc software library (Balay 2017). Acoustic point sources as well as source surfaces with given pressure and velocity values can be used. The code is parallelized using the OpenMPI application programming interface.

2.2 Experimental Verification

For the investigation of the noise shielding properties of generic bodies or aircraft configurations, it is necessary to utilize a reference sound source with known characteristics (i.e., known directivity and spectral content). Such a source can be realized using a conventional loudspeaker or, as in Hutcheson (2014), using customized pipe arrangements and pressurized air. However, the physical dimensions of these sources make their use in aeroacoustic investigations difficult because they interfere directly with the flow field and/or the acoustic field, thus adding perturbation to any acoustic measurement.

A laser-based (non-intrusive) pulsed sound source was specially developed for the experiments. By focusing a high energy laser beam to a point (i.e., an effective air volume), it is possible to initiate the formation of a small plasma, which rapidly expands (Hosoya 2013), thus forming a pressure wave about its boundary, which propagates through the surrounding medium. This source circumvents all the above inconvenient while providing a reference acoustic pressure wave of nearly uniform directivity with broadband spectral content. Because of its very short pulse duration, the generated sound wave also has the advantage of being easily separated from unwanted reflection. Furthermore, its characteristics can be derived directly from the solution of the acoustic wave equations, making its implementation in numerical simulation codes straightforward (Rossignol 2015).

The setup described above had to be modified to make sure that the laser beam, past the focus point, did not interact with the surface of the model. Because the source had to be placed at about 20 mm from the model surface, the laser beam, past the focal point, was found to produce local explosions on the model's surface. To avoid this issue, a mirror had to be installed at a 45° angle to the laser beam path to deflect the beam and make it follow a path parallel to the tunnel x axis (i.e. in streamwise direction). This modification to the setup made it no longer possible to conduct experiments with the wind tunnel running (i.e. data are available only for a Mach number of M=0). The source position selected for the investigations are shown in Fig. 5. Details of the laser source setup, acquisition chain and data processing are not repeated here. The interested reader can find more information in Rossignol (2017).

The wind tunnel model selected for testing is DLR's SACCON model (see Figure 1). Details of the SACCON geometry are shown in Figure 1. The model is shown in its configuration with intake and exhaust openings. For the wind tunnel campaign, however, the model tested had a slick upper side, without opening. This implies that sound wave diffraction inside the engine channel was not considered in the investigations. The experimental setup is shown in Figure 2. In that picture, the whole test section of the DNW-NWB is visible as seen from the tunnel's nozzle. The coordinate system definition is indicated in Figure 2.

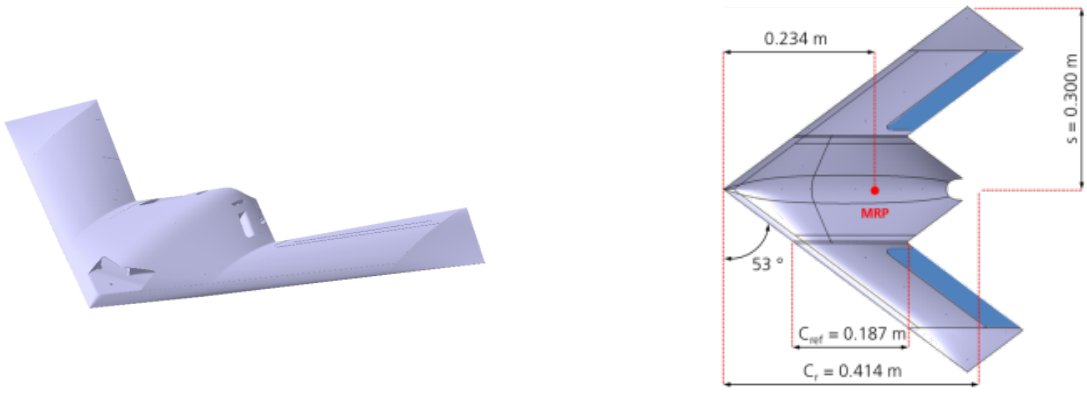

Figure 1: SACCON UCAV model, MRP = Moment Reference Point

In Figure 2, the SACCON model can be seen in the middle of the test setup, held in place in a vertical fashion and at angle of attack α=0°, using a sting support. The upper side of the model points towards the right-hand-side of the picture. On the left-hand-side of Figure 2, four free-field microphones and three in-flow microphones were installed to acquire the acoustic field below the model's lower surface, equivalent to a measurement below the flight path of the aircraft. The three in-flow microphones were mounted to a single axis linear displacement system to achieve measurements over the largest possible range of streamwise positions. The optical components needed to generate the sound source and the positioning system are located on the RHS of Figure 2. Two free-field microphones were fixed outside of the tunnel jet, to monitor the reference acoustic source amplitude versus time over the course of the measurement campaign. The set of source positions available in the database is depicted in Figure 3.

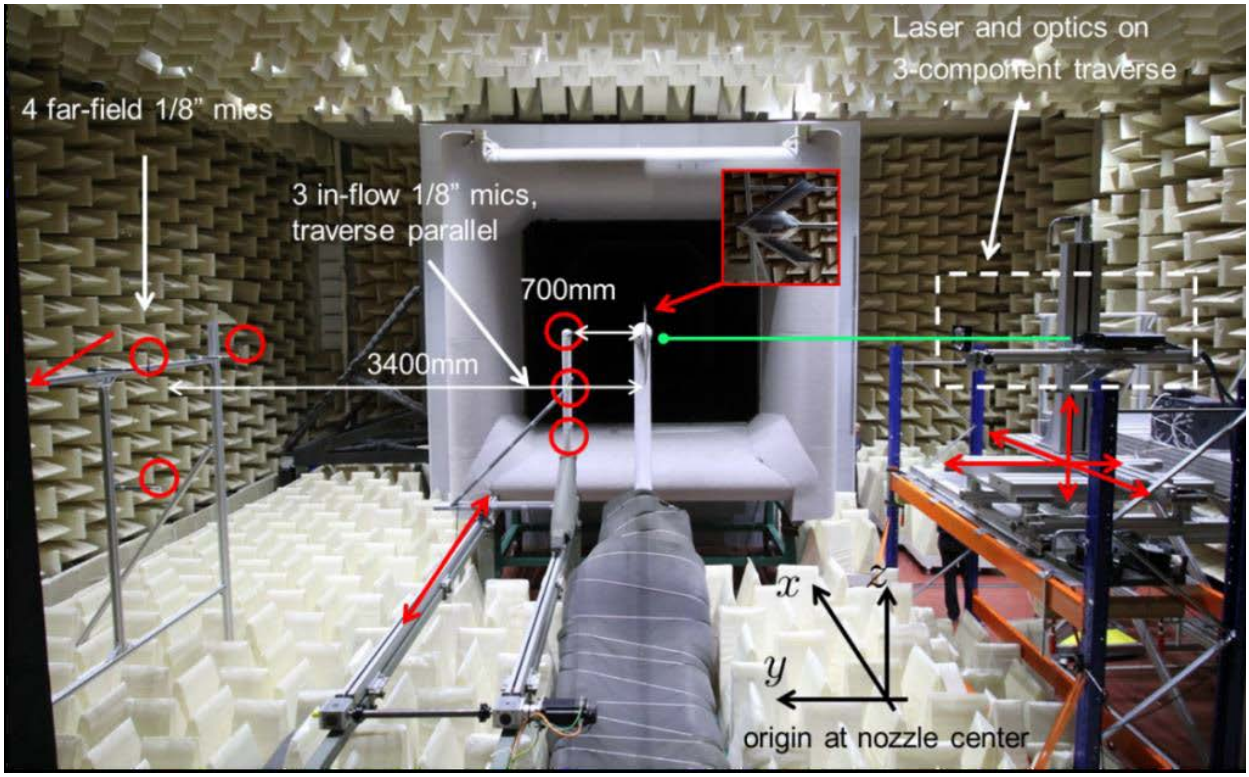

Figure 2: Experimental setup in the DNW-NWB wind tunnel

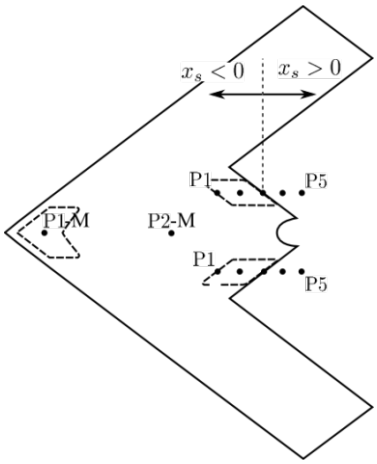

Figure 3: Selected source positions relative for the experiment

2.3 Results

2.3.1 Data analysis and presentation

Standard quantities are defined for the quantification of the shielding efficiency of the test wing. If not otherwise mentioned, the results will be given in terms of "*octave-band normalized shielding levels*",

$$\gamma^n_{p(1/1)}(f_c) = 20\log\left(\eta^n_{(1/1)}\right) \tag{1}$$

The narrow band spectrum of the shielding factor $\eta(f)$ is defined as,

$$\eta(f) = \frac{|\hat{p}^r_s|}{|\hat{p}^r_i|} = \frac{|\hat{p}_s|}{|\hat{p}_i|} = \sqrt{\frac{\mathrm{PSD}^r_s}{\mathrm{PSD}^r_i}} = \sqrt{\frac{\mathrm{PSD}_s}{\mathrm{PSD}_i}} \tag{2}$$

where $\hat{p}(f)$ stands for the Fourier coefficients of the Fourier-transformed pulses. From $\hat{p}(f)$ we determine octave band averages of the shielding factor $\eta^n_{(1/1)}(f_c)$ (see Eq. 5) for $f_c = 7$ kHz, 14 kHz, 28 kHz.

$$\eta^n_{(1/1)}(f_c) = \left(\frac{\sqrt{2}}{f_c}\int_{f_c/\sqrt{2}}^{f_c\sqrt{2}} \eta^2(f)df\right)^{1/2} \tag{3}$$

The motivation behind the use of octave-band average values of the shielding factor is to produce curves that are less oscillatory and therefore more easily interpretable and comparable between experiments. The unconventional choice of octave band central frequencies is motivated by the characteristics of the source which radiates with maximum energy at about 28 kHz. The frequency-wise determination of the shielding factors ensures that the results will be independent of the source frequency content. In Figure 4 typical spectra of the incident sound pressure, $\hat{p}_i$, the attenuated pressure $\hat{p}_s$ and of the shielding factor $\eta(f)$ are plotted.

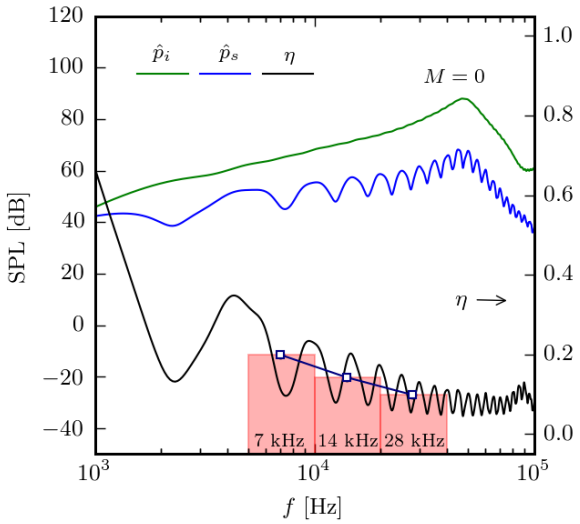

Figure 4: Spectra of the incident, $\hat{p}_i$, and shielded, $\hat{p}_s$, pressures waves and shielding factor η, M=0, $\Delta f = 61$ Hz. Octave bands and respective average value of η shown by shaded area and empty square symbols.

The oscillatory character of the attenuated pressure and of the shielding factor spectra is a consequence of sound scattering by the model. The octave bands considered in the analysis are also shown by the areas shaded in red. Higher octave band frequencies are not considered in the analysis because the source wave amplitude was found to be affected by non-linear propagation effects, thus rendering biased shielding levels (Rossignol 2018).

2.3.2 Shielding level vs. observer position

In the following, the shadow zone refers to the zone where no direct line of sight exists between the acoustic source and a specific microphone. The results of the experiments for six source positions as a function of the observer position are summarized in the plots of Figure 5. First, looking at the most downstream source positions, for all octave bands, shielding is close to none, as expected. The spreading observed in the curves of Figure 5 at P4 and P5 is most probably related to the close proximity of the sting to the source, as well as to reflections on the rear part of the model which cannot be properly distinguished in post-processing. The reference, unshielded pressures used to compute the shielding factors being acquired in the empty test section. Moving to source positions P2 and P3, one can observe a progressive increase in sound attenuation. At P3 where the source is directly above the aircraft's trailing edge (i.e. $x_s - x_{TE} = 0$), most of the shielding occurs upstream of the trailing edge while downstream the curves tend to zero. For P2, now the source is upstream of the trailing edge and a strong attenuation of up to -16 dB is registered at the most upstream measurement position. These observations also hold at P1 with even larger attenuations, up to -24 dB at the most upstream measurement position and for the 28 kHz octave band. The shielding levels are a function of the octave band frequency considered, sound wave attenuation increasing with an increase in octave band frequency. This is a known effect deduced in the classical geometrical diffraction theory (Keller 1962). Sound wave diffraction at a trailing edge is a function of the incident wave wavenumber and of the diffracting edge dimensions.

At position P1M in Figure 5, i.e. a source at the engine intake position, even if the microphone is kept in the shadow zone the attenuation is almost 15 dB less, compared to what is observed for a source at P1, for the 28 kHz octave band. At P1-M, all octave bands display lower attenuation levels compared results at source position P1. A stronger dependency of the results on the incident sound wavelength is observed, compared to other source positions, an indication that sound wave diffraction at the curved leading edge of the aircraft, may be more important than at the trailing edge. Also, the geometrical symmetry of the aircraft promotes sound

wave amplification below the flight path. This result emphasizes the potential loss in overall noise shielding which could occur for a noisy intake, even with a careful placement of the engine outlet. Note, however, that in the present experiment the intake and outlet noise contributions are assumed to be equal in power, through the experimental methodology. The actual source ranking between intake and outlet is not known and cannot be derived from the above results. This aspect will need to be addressed in future research efforts.

2.3.3 Comparison with simulation results

A comparison of simulation results with the measurement data is given in Figure 6. The comparison is done based on contour plots of the shielding level for a narrow-band ($\Delta f = 61$ Hz) frequency of 28 kHz. The source position is shown by the red dot, it corresponds to position P2. The experimental results are shown in the first row, where the "+" correspond to the actual microphone positions. The simulation results are shown in the second row for the same frequency, and virtual microphone positions. In this row, the simulation data were down-sampled to match the spatial resolution of the experimental data (depicted by the "+"). The simulation data are found to be in satisfactory agreement with the experiment. Local deviations in the contours may be seen. Quite small deviations of the sensor positions from their nominal values may let it pick up e.g. a local maximum inside of a narrow interference fringe pattern, while on the desired position there may just be a local minimum. Also, note that the extent of the computational domain is slightly smaller than in the experiment and is limited to x=1 m in streamwise direction.

A comparison between the measured and simulated narrow band shielding levels for 7 kHz and 28 kHz is presented in Figure 7 for source positions P1 and P1M below the flightpath. The results of Figure 7 are consistent with the trends previously observed in Figure 5, for the same source positions. The simulation results are plotted using solid lines while the measured data are plotted using dashed lines with solid dots. The resolution of the simulation results in this figure is higher compared to the experimental data.

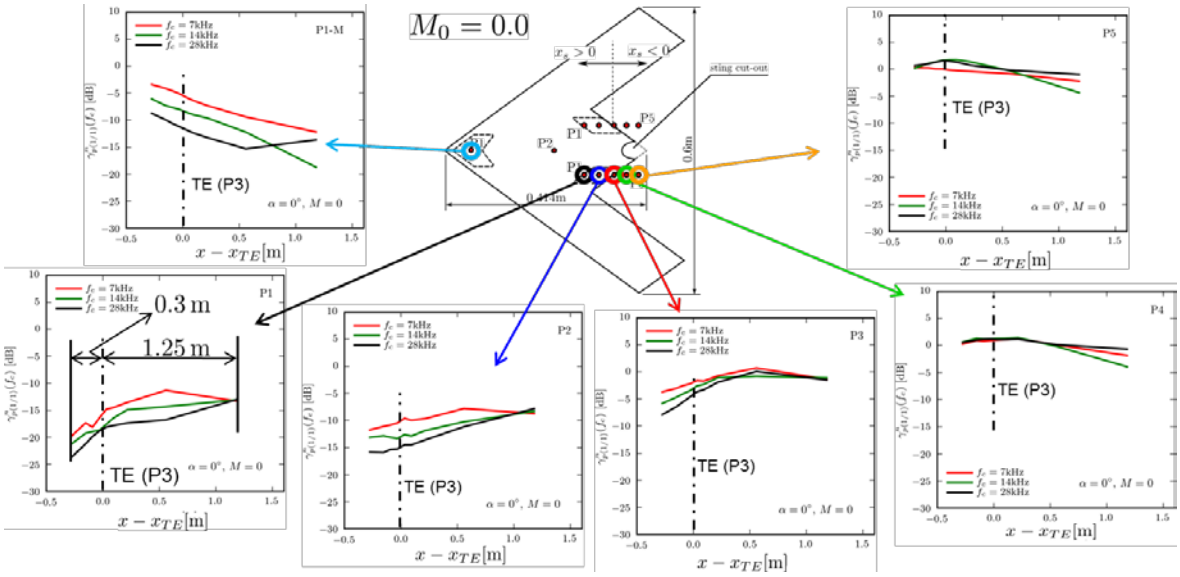

Figure 5: Octave band shielding level vs. source position and observer location below the flight path

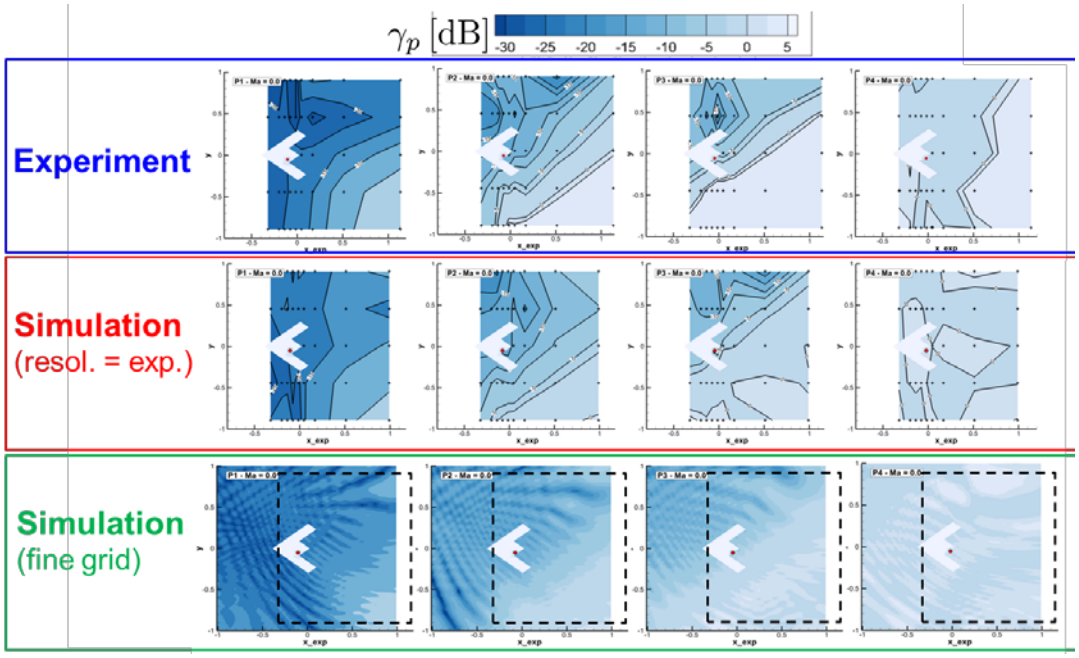

Figure 6: Contours of shielding levels. Experiment vs. simulation. 28 kHz

In the experiment, only nine microphones positions are available. The simulations data show much more wiggles, details which cannot be revealed by the measurements, at this spatial resolution. Nonetheless, both simulations and measurements reveal similar trends and are in good agreement. The important reduction in attenuation identified in Figure 5 for source position P1-M, is also observed in the simulation results. This comparison lends further support to the conclusion made above regarding the importance of a well-thought design of the intake to ensure high overall noise attenuation and, therefore, a low detectability of UCAV's. The above comparison of the simulation results against the experimental data supports the capabilities of the FMCAS code.

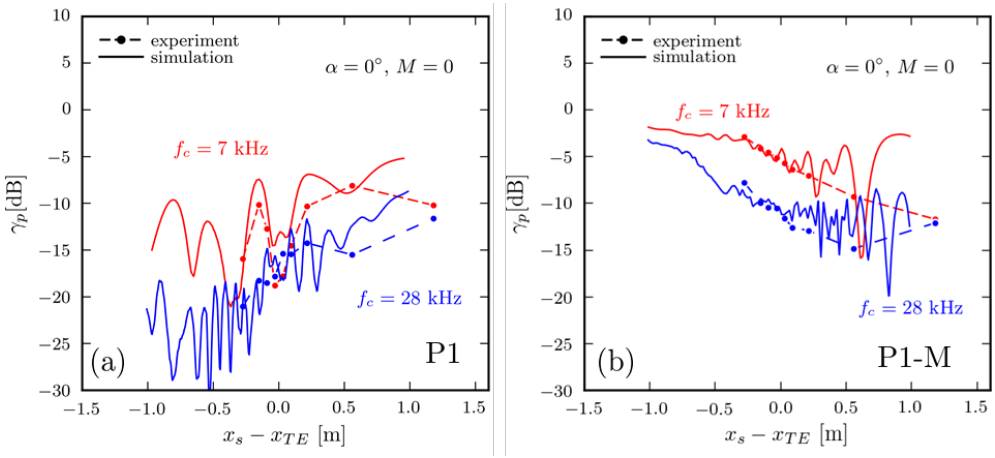

Figure 7: Comparison of measured and simulated narrow band shielding levels at the fly-over position (R=0.7 m) for 7 kHz (red) and 28 kHz (blue). Experiment: dashed line with solid dots, simulations solid lines. $\Delta f = 61$ Hz

3.0 ACOUSTIC SIGNATURE ASSESSMENT OF MULDICON

The SACCON studies have shown the applicability of the BEM method for the generic assessment of the acoustic shielding characteristics of an agile unmanned combat aircraft configuration. However, for real highly-integrated propulsion systems, noise radiation from intake and exhaust is critical to the acoustic detectability of an aircraft, especially to low-observable configuration. Assessing the noise signature of a UCAV configuration at an early design stage would be therefore more effective than any late stage adaption of the design. The methodology used for the assessment should be able to account for mean flow effects on noise generation and propagation. Noise radiation from the intake can be significantly affected by the flow deviation inside the intake duct, while the jet can critically interact with the airframe and generate additional noise sources. These aspects were not considered in the assessment of the SACCON and require further experimental and numerical investigations. In this section DLR-F24 MULDICON UCAV is introduced, along with numerical simulations results aimed at providing first insights into the aeroacoustics of a realistic agile UCAV configuration.

3.1 DLR-F24 MULDICON UCAV configuration

The original MULDICON configuration was developed in the framework of NATO STO Task Group AVT-251 (Conceptual UCAV Design). The aim of this Task Group was to perform an aerodynamic re-design of the SACCON UCAV, only through the use of flow simulations methods i.e. CFD. This was made possible through knowledge gained throughout earlier Task Groups. In AVT-161, the ability of computational methods to accurately predict static and dynamic stability was evaluated. The AVT-201 task group aimed at including control surfaces in the aerodynamic assessment as well as investigating ways to perform full flight simulations (Cummings 2018). AVT-251 was not about designing a competitive UCAV but rather aimed at improving SACCON while making it a realistic, flyable, vehicle. To achieve this goal SACCON was first evaluated with respect to its ability to fulfil a flight mission, i.e. prescribed flight trajectory at a given altitude of 11 km and Mach number of 0.8 for a given payload (Cummings 2018). The result of this evaluation emphasized the poor control characteristics of SACCON, due to the high-sweep design of its trailing edges. This led the group to design a new configuration, MULDICON, circumventing the issues encountered with SACCON.

In the framework of Task Group AVT-318 (Low noise aeroacoustic design for turbofan powered NATO air vehicles), it is intended to pursue the work started in Task Group AVT-233 (Aeroacoustics of Engine Installation on Military Air Vehicles) to now deal with realistic sources on a concurrent agile (unmanned) NATO air vehicle design.

The objectives of AVT-318 are,

1. Demonstrate qualification and applicability of numerical tools for the prediction of realistic propulsion system installation on received sound
2. Evaluate the prediction of noise reduction technology as an exercise in aeroacoustic design at agile NATO air vehicles
3. Conduct a benchmark exercise among partners
4. Provide a dedicated aeroacoustic validation dataset from acoustic wind tunnel tests

The original MULDICON UCAV planform, from AVT-251, was adopted for the experiments in AVT-318 and modified to allow the integration of an intake and an exhaust channel, as depicted in Figure 8. The original planform remained untouched while the center body design by FOI (Swedish Defense Research Agency) was selected (Edefur 2018). This design has a thicker center body, leaving more room for the intake and exhaust channels integration. This version of the model is referenced to as DLR-F24 MULDICON UCAV.

It was specifically design for testing in the acoustics test section of the low-speed acoustic wind tunnel of DNW in Braunschweig (DNW-NWB). The design allows for the realization of a controlled high-velocity intake flow as well as a cold high-velocity exhaust jet. This will allow for thorough investigations of the acoustic signature of the DLR-F24 MULDICON UCAV. An overview of the experimental setup is given in Figure 9.

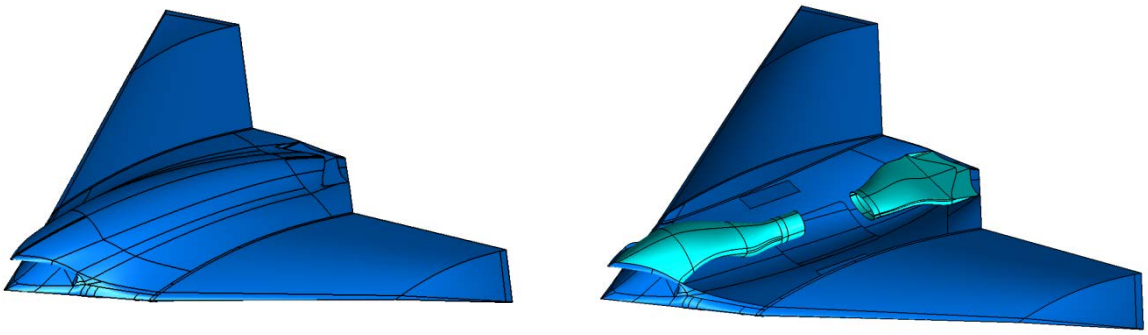

(a) DLR F-24 MULDICON UCAV **(b) Intake and exhaust ducts**

Figure 8: DLR-F24 MULDICON UCAV configuration

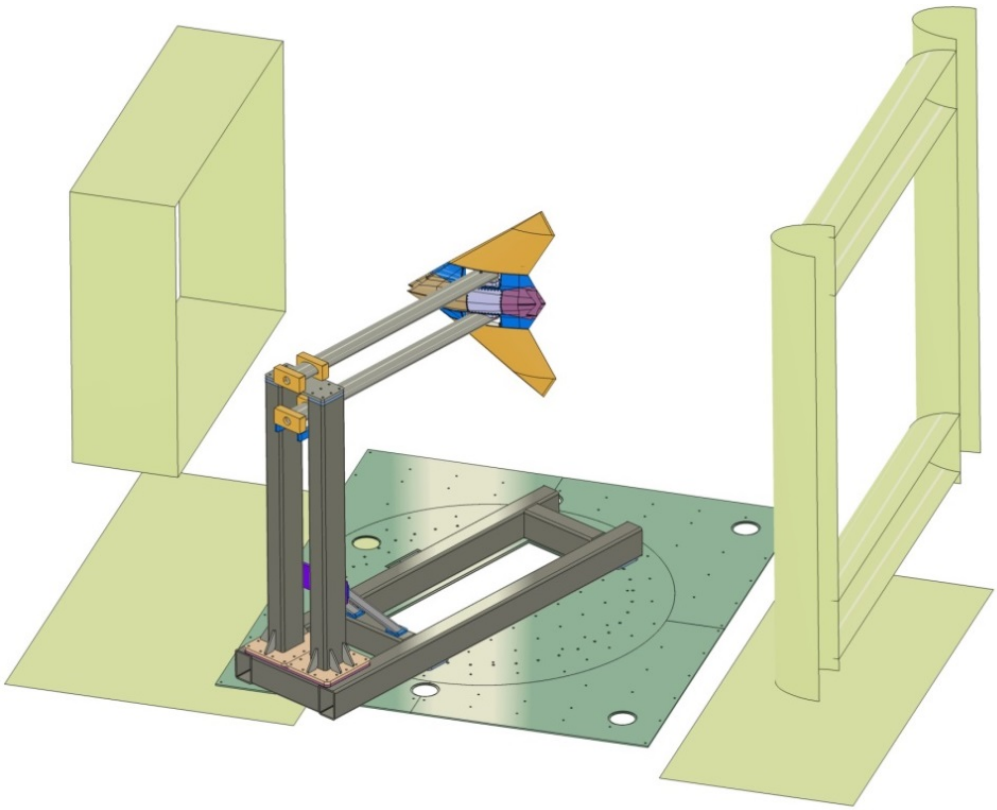

Figure 9: Planned experimental setup in the anechoic test section of DNW-NWB

3.2 Near-Field Coupling Simulation Method

Numerical methods and procedures undertaken for evaluating intake and exhaust radiated noise of a UCAV configuration can be summarized as follows. For intake noise predictions, the rotating fan blades give rise to acoustic modes which are propagated out of the intake duct in a RANS mean flow using a volume resolving Discontinuous Galerkin (DG) method. A coupled simulation approach is undertaken for acoustic predictions where the entire UCAV aircraft surface is taken into consideration by means of the Fast-Multipole Boundary Element Method (FM-BEM) which accounts for sound shielding and scattering up to a far-field observer. The exhaust noise sources which originate due to a jet - plate interaction are simulated with the Fast Random Particle Mesh (FRPM) method (Neifeld 2015; Mößner 2018) and in the near-field region the acoustic wave propagation is computed by the DG DISCO++ solver in the time domain (Ffwocs Willams 1969). In contrary to propagating fan modes, jet interaction noise is computed in the time domain due to the broadband nature of acoustic sources. Figure 10 depicts an overview of noise propagation techniques employed in this work.

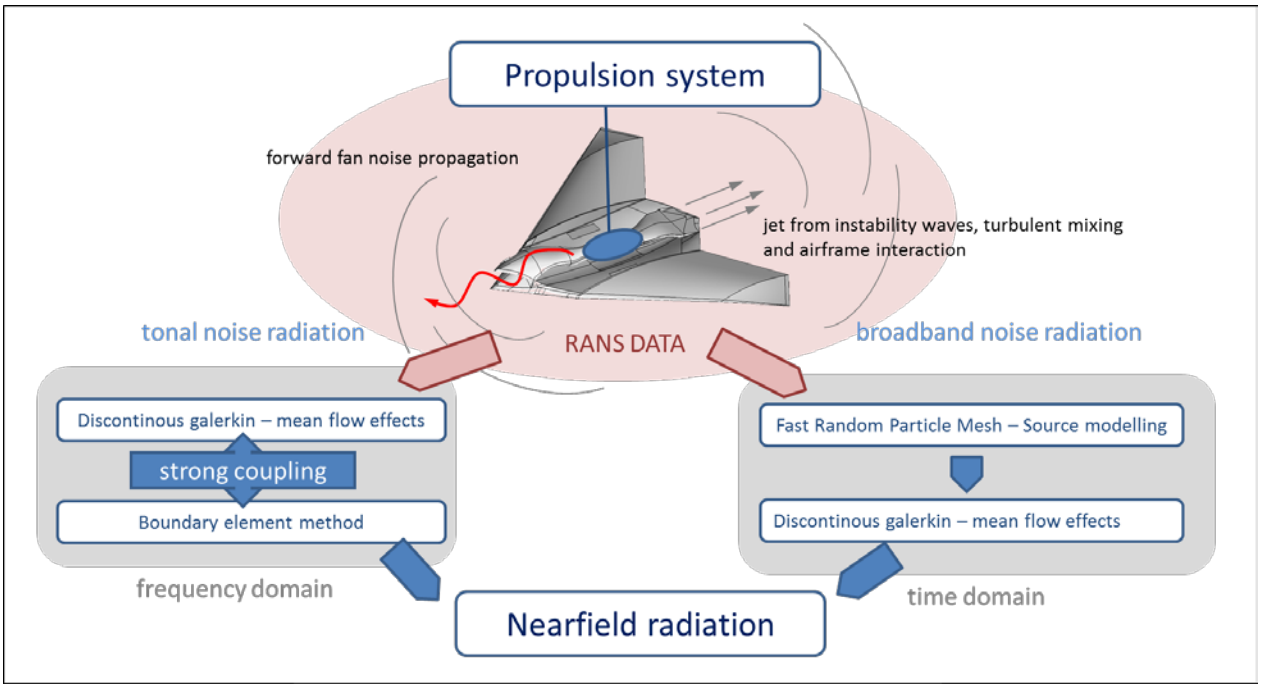

Figure 10: Overview on acoustic propagation methods

3.2.1 Intake rotating modes and jet interaction noise

Numerical results are provided as a proof of concept for the noise radiated from the MULDICON configuration. First, in Section 3.2.2 the simulation results for noise radiated from the intake are presented. Second, the results for jet trailing edge noise interaction are provided in Section 3.2.3.

3.2.2 Intake radiation

Figure 11(a) shows the real part of acoustic pressure contour obtained by solving the wave propagation with DG. The UCAV intake is surrounded by a spherical coupling surface as shown in Figure 11(b). Notice that only a mere fraction of the entire domain is occupied by the computationally expensive DG region. This results in significant computational savings but without a significant decrease in noise prediction quality thanks to the efficient FMBEM which is applied beyond the coupling surface within its region of validity of nearly potential flow. The feedback from the FMBEM is used to prescribe global boundary conditions onto the DG region. Here the two-way information exchange is essential for obtaining accurate sound radiation.

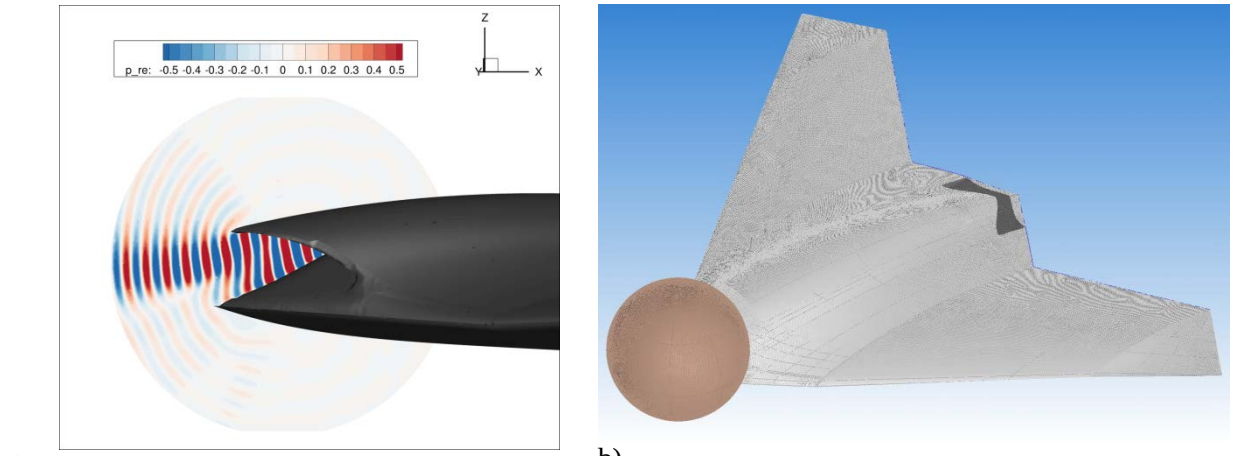

a) b)

Figure 11: Acoustic pressure fluctuations propagated from the intake (a), FMBEM surface mesh with a spherical coupling surface over the intake (b).

The rotating modes were prescribed for two frequencies of interest, 5 kHz and 10 kHz. These frequencies are selected because they can be easily excited in the wind tunnel experiment. The initial simulations were

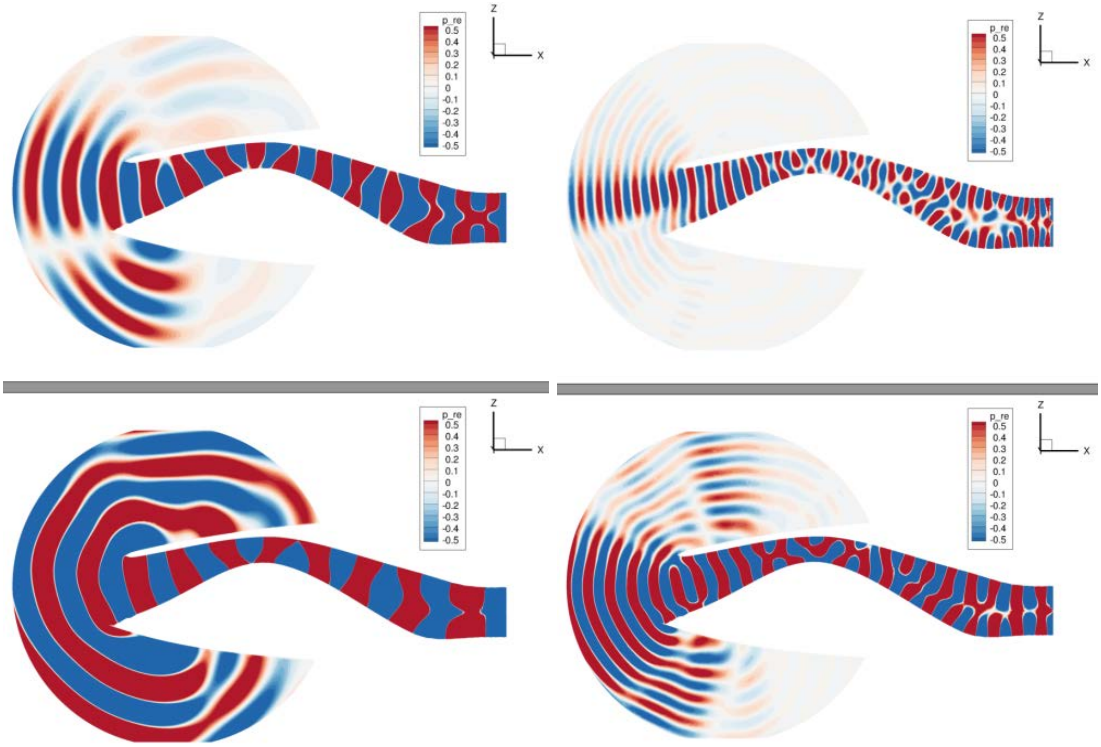

Figure 12: Acoustic wave propagation in the intake duct, 5 kHz (left) and 10 kHz (right), with flow (top), without flow (bottom)

performed without the background flow and compared to the wave propagation computed in the RANS flow. The differences are well visible in Figure 12 where not only the acoustic frequency but also the radiation pattern changes significantly due to a high Ma number intake flow. The trend is similar for both frequencies where stronger radiation is found without the added flow. At present, the outgoing frequency (from DG to FMBEM) was not corrected for the Ma number. This can have an effect on shielding and directivities. The free stream Ma number was 0.175 in both cases which is considered low and still within the validity region of the FMBEM.

The sound directivity was computed at a 6 m radius from the origin, i.e. at the intake lower lip tip in Figure 12, with 360 numerical microphones wrapped around y-axis. Figure 13 shows SPL levels with the flow convection taken into account. These were derived from a coupled DG to FMBEM solutions corresponding to the top contours in Figure 12.

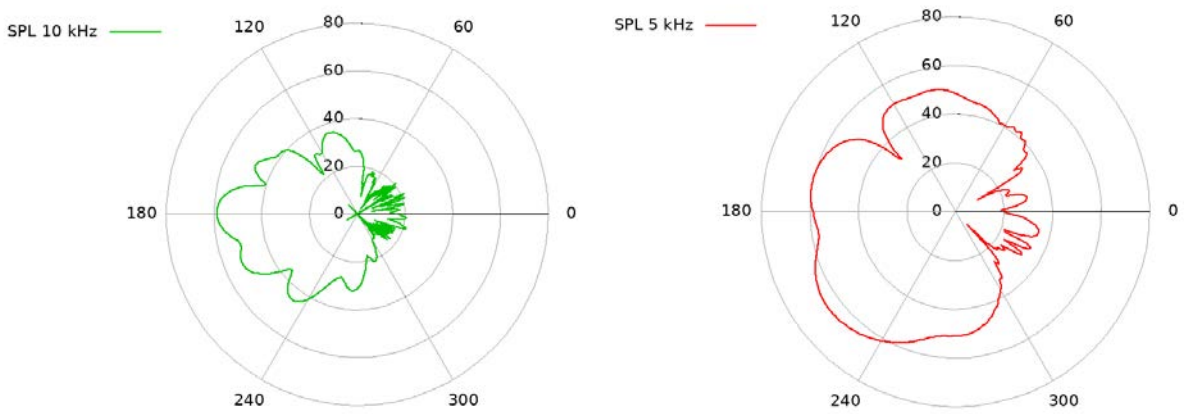

Figure 13: Sound pressure directivity plots for two different frequencies 10kHz (left) and 5kHz (right), with added mean flow, Ma=0.175

It is evident that for the current UCAV design the acoustic radiation is predominantly upstream in the direction towards the ground judging from the highest SPL levels in Figure 13. The amplitude of the signal tends to decrease with increasing frequency. Also, with increasing Ma number inside the intake duct one should expect to see a decrease in fan noise measured in the far-field.

3.2.3 Jet interaction noise

The installed exhaust configuration may trigger different noise mechanisms. The focus of this work is specifically on the interaction of the jet with an airframe trailing edge. The noise sources which are expected to originate predominantly in the region of the potential core of a thin elliptic jet are modelled with the stochastic FRPM method. The sources are then propagated by means of a volume resolving DG method up to a distant Ffowcs-Williams and Hawkings (FW-H) surface (Ffwocs Willams 1969) and finally, the noise is integrated to a far-field observer. So far a preliminary stage showing the instantaneous contour of acoustic pressure is depicted in Figure 14. Our approach closely follows the guidelines of a calibrated method used for predicting jet interaction noise with the FRPM method (Blech 2020; Neifeld 2015). In Figure 14, the instantaneous acoustic pressure field near the exhaust is shown on a slice through the symmetry plane of the domain. The presence of the wing's trailing edge in the vicinity of the jet leads to wave propagation with a dominant forward arc directivity at low-frequency. This effect is clearly of high-relevance with respect to the choice of an appropriate noise mitigation concept.

3.3 Future work

Upcoming experimental work on the DLR-F24 Muldicon model will focus on a parametric quantification of fly-over intake and exhaust noise radiation, as well as overall airframe noise. Furthermore it is intended to investigate ways to reduce noise emission towards the ground. This includes concepts related to geometric modifications at the intake and exhaust as well as the application of passive noise reduction technologies, e.g. porous material inserts. The methodology presented in this contribution aims, in part, at numerically replicating results from the low-speed wind tunnel experiments. To this end the focus is put on low Mach, number free-stream conditions i.e. M=0.178.

The generic mission defined in AVT-251 (Cummings 2018) requires a mission flight Mach number of 0.8 over most of its range. The numerical coupling described in this paper is, however, formulated for the noise sources in a low-Mach number background flow. Simulations at a flight Mach number of 0.8 would require a change of numerical methodology which is outside the scope of the current effort. One can expect forward radiating fan noise to decrease with the increasing Mach number where at cruise conditions (Ma of 0.8) and high altitude the noise signature is expected to be negligible. Concerning the exhaust noise, realistic jet Mach numbers are already factored into the current experimental and numerical simulation campaigns. At present, only a cold jet is considered due to wind tunnel testing capabilities.

Therefore, for the future design optimisation of UCAV configurations with acoustics in mind our focus remains on improving noise prediction methods at low flight Mach numbers. The numerical simulation results will provide valuable insights into how to maximize acoustic shielding through geometric design and how to minimize noise from unfavourable installation effects; knowledge which will be transferable to higher flight Mach number conditions.

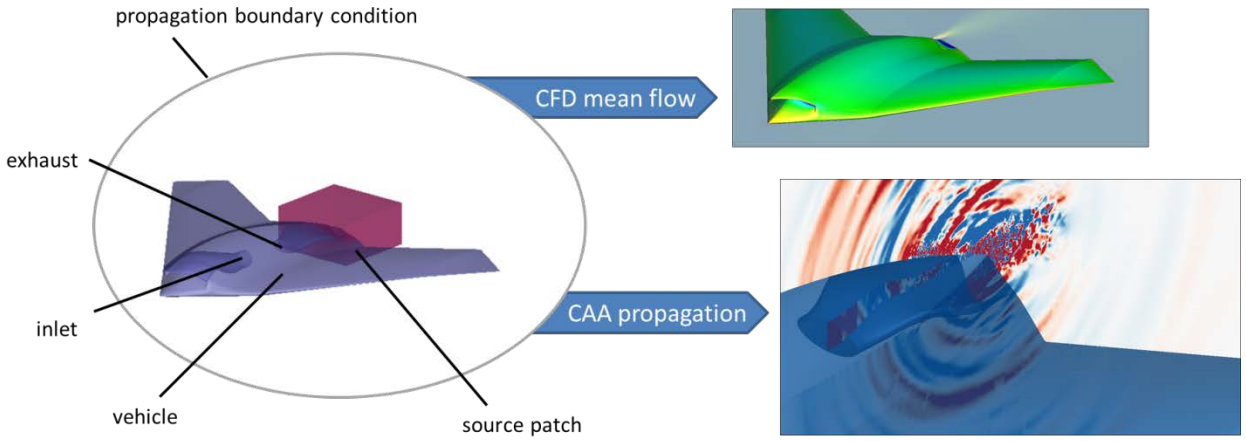

Figure 14: Overview on CFD mean flow and instantaneous CAA propagation using FRPM sources derived from CFD turbulence parameters

4.0 CONCLUSIONS

An application of the BEM method for the generic assessment of the acoustic shielding characteristics of an agile unmanned combat aircraft configuration, the SACCON (Cummings 2018) is presented. The numerical simulations were backed by a wind tunnel experiment using a laser based monopole-like sound source as a generic engine model. The experiment was conducted in the low-speed acoustic wind tunnel, DNW-NWB, in Braunschweig. The acoustic shielding characteristics of SACCON, were investigated in terms of their dependency on source placement and frequency.

The results reveal that octave band shielding levels as high as -25 dB can be achieved for the source positions furthest upstream of the trailing edge. Slight position shifts toward the trailing edge have a large impact on the overall attenuation. Also, attenuation is a strong function of frequency, with higher frequencies being more attenuated in the shadow zone. This can be related to the sharp-edges of the model, relative to the sound wavelength, which leads to a sharply defined shadow zone. In comparison, for wavelength comparable to the radius or thickness of the edge, a stronger diffraction of the sound about the edge into the shadow zone will occur, leading to less attenuation.

It was also recognized that noise generated at the engine intake is much less attenuated. This is a consequence of the position of the inlet, centered on the symmetry plane of the model as well as to the relatively large radius of curvature of the aircraft wings leading edge. Inlet generated noise is registered, in the experiments, far downstream of the aircraft leading edge. This result emphasizes the potential necessity to achieve an acoustically optimized integration of both intake and exhaust altogether to maximize acoustic attenuation. A ranking of both sources, i.e. intake vs. exhaust, could not, however, be done using the acquired database. This question remains open and will be the subject of future research.

Validations of simulations done using DLR's FMCAS code were performed and a satisfactory agreement between simulation and experiment was found. The added insight provided by the numerical simulations will help in better understanding the shielding problem and therefore, allow the design of a more silent UCAV.

Although the laser-based sound source provides excellent means to assess shielding effects in a generic manner, it does not allow for an evaluation of real highly-integrated propulsion systems. For such systems, noise radiation from the intake and exhaust is critical to the acoustic detection of an aircraft, especially to low-observable configurations. Aiming at an assessment of the noise signature of a realistic UCAV configuration at an early design stage, experimental and numerical methodologies are presented which are able to account for mean flow and airframe interaction effects on noise generation and propagation. Finally, the DLR-F24 MULDICON UCAV test bed is introduced which allows for the realization of a controlled high-velocity intake flow as well as a cold high-velocity exhaust jet. Thus, providing means for a thorough investigation of the acoustic signature of a realistic UCAV configuration.

The incremental steps described in this contribution are necessary to demonstrate the qualification of current methodologies for the aeroacoustic assessment of low-Observable UCAV configurations. This will ultimately enable the aeroacoustic assessment to be part of the early design phase of such vehicles, a goal already clearly formulated in the framework of AVT-251 (Cummings 2018).

5.0 REFERENCES

Balay, S. & Abhyankar, S., (2018). *"PETSc User Manual"*, s.l.: Argonne National Laboratory, ANL-95/11 – Revision 3.8.

Blech, C. et al., (2020). "Numerical prediction of passenger cabin noise due to jet noise by an ultra–high–bypass ratio engine". *Journal of Sound and Vibration*, Volume 464.

Cummings, R. M., Liersch, C. M. & Schütte, A., (2018). *"Multi-Disciplinary Design and Performance Assessment of Effective, Agile NATO Air Vehicles"*. Atlanta, USA, AIAA Applied Aerodynamics Conference.

Czech, M. J., Thomas, R. H. & and Elkoby, R., (2012). "Propulsion airframe aeroacoustic integration effects for a hybrid wing body aircraft configuration". *International Journal of Aeroacoustics*, 11(3-4), pp. 335-367.

Edefur, H. & Tormalm, M. H., (2018). *"Design and Integration of a Low Observable Intake for the MULDICON Platform"*. Atlanta, USA, AIAA Applied Aerodynamics Conference.

Ffowcs Williams, J. E. & Hawkings, D. L., "1969). "Sound generation by turbulence and surfaces in arbitrary motion". *Philosophical Transactions of the Royal Society of London. Series A, Mathematical and Physical Sciences*, 264(1151), pp. 321-342.

Hosoya, N., Nagata, M. & Kajiwara, I., (2013). "Acoustic testing in a very small space based on a point sound source generated by laser-induced breakdown: Stabilization of plasma formation". *Journal of Sound and Vibration*, 332(19), pp. 4572-4583.

Hutcheson, F. V. et al., (2016). *"Shielding of Turbomachinery Broadband Noise from a Hybrid wing Body Aircraft Configuration"*. Lyon, France, 22nd AIAA/CEAS Aeroacoustics Conference.

Keller, J. B., (1962). "Geometrical theory of diffraction". *JOSA 52.2*, pp. 116-130.

Mößner, M., Delfs, J., Kissner, C. & Enghardt, L., (2018). *"Computational chain for virtual fly-over simulations applied to fan noise"*. Atlanta, USA, 24th AIAA/CEAS Aeroacoustics Conference.

Neifeld, A., Boenke, D., Dierke, J. & Ewert, R., (2015). *"Jet noise prediction with eddy relaxation source model"*. Dallas, USA, 21th AIAA/CEAS Aeroacoustics Conference.

Papamoschou, D. & Mayoral, S., (2009). *"Experiments on shielding of jet noise by airframe surfaces"*. Miami, USA, 15th AIAA/CEAS Aeroacoustics Conference.

Rahola, J., (1998). "Diagonal forms of the translation operators in the fast multipole algorithm for scattering problems". *BIT Numerical Mathematics*, 36(2), pp. 333-358.

Rossignol, K.-S. & Delfs, J. W., (2016). *"Analysis of the Noise Shielding Characteristics of a NACA0012 2D Wing"*. Lyon, France, 22nd AIAA/CEAS Aeroacoustics Conference.

Rossignol, K.-S., Delfs, J. W. & Boden, F., (2015). *"On the Relevance of Convection Effects for a Laser-Generated Sound Source"*. Dallas, USA, 21st AIAA/CEAS Aeroacoustics Conference.

Rossignol, K.-S.et al., (2018). *"Experimental Investigations on Noise Shielding: Dependency on Reference Noise Source and Testing Environment"*. Atlanta, USA, 24th AIAA/CEAS Aeroacoustics Conference.

Rossignol, K.-S.et al., (2017). *"Investigating Noise Shielding by Unconventional Aircraft Configurations"*. Denver, USA, 23rd AIAA/CEAS Aeroacoustics Conference.